pp 1170–1189.
doi:10.1017/aer.2020.22

Coordinated control of fuel flow rate and air flow rate of a supersonic heat-airflow simulated test system

C. Cai L. Guo and J. Liu
caichaozhi1983@163.com
School of Mechanical and Equipment Engineering
Hebei University of Engineering
Handan, Hebei
China

ABSTRACT

The gas temperature of the supersonic heat airflow simulated test system is mainly determined by the fuel and air flow rates which enter the system combustor. In order to realise a high-quality control of gas temperature, in addition to maintaining the optimum ratio of fuel and air flow rates, the dynamic characteristics of them in the combustion process are also required to be synchronised. Aiming at the coordinated control problem of fuel and air flow rates, the mathematical models of fuel and air supply subsystems are established, and the characteristics of the systems are analysed. According to the characteristics of the systems and the requirements of coordinated control, a fuzzy-PI cross-coupling coordinated control strategy based on neural sliding mode predictive control is proposed. On this basis, the proposed control algorithm is simulated and experimentally studied. The results show that the proposed control algorithm has good control performance. It cannot only realise the accurate control of fuel flow rate and air flow rate, but also realise the coordinated control of the two.

Keywords: Supersonic; fuel flow rate; air flow rate; neural sliding mode predictive control; coordinated control

NOMENCLATURE

q_f	the theoretical fuel flow rate
K_f	the gain between the frequency and the control voltage
m_p	number of the motor pole pairs
J_T	the rotational inertia of the motor shaft
D_p	displacement of the pump

Received 23 August 2019; revised 14 January 2020; accepted 7 February 2020.

C_{p} the whole leakage coefficient
R_{L} liquid resistance of the pipeline
l the length of the pipeline
ρ_f the fuel density
C_{d} flow coefficient of the nozzle
p_2^* the operating spout pressure
τ time delay of fuel supply subsystem
K_{s1} the amplification gain of the servo valve
x_v the displacement of the servo valve
T_v the time constant of the servo valve
K_c the flow pressure coefficient
Q_L the load flow rate
C_t the total leakage coefficient
V_t the volume of the cylinder block
B_p the viscous damping coefficient
F_L the external load force
ω_h the hydraulic natural frequency
K_{ce} the total pressure and flow coefficient including leakage
w the gradient of the opening area of the valve
p the pressure of the combustor
k the isentropic index
q_a the air mass flow rate
u_s the input voltage of the electro-hydraulic servo valve amplifier
u the control voltage
K_{int} the voltage-frequency ratio
R_{re} equivalent resistance of the rotor
B_{T} damping coefficient of the motor shaft
η_{m} the mechanical efficiency of the pump
L liquid inductance
R_{N} liquid resistance of the nozzle
d the diameter of the pipeline
μ the dynamic viscosity of the fuel
A_0 the cross-sectional area of the nozzle
q_{sf} the actual fuel flow rate
I the driving current of the servo valve
u_s the input voltage of the servo amplifier
K_{s2} the displacement driving coefficient of the servo valve
K_{sq} the flow coefficient
p_L the load pressure
A_p the cross-section area of the hydraulic cylinder
x_p the displacement of the piston of the hydraulic cylinder
β_e the bulk elastic modulus

https://doi.org/10.1017/aer.2020.22 Published online by Cambridge University Press

M_t	the mass of the cylinder block
k_1	the spring stiffness
ζ_h	the damping ratio
C_{d1}	the flow coefficient of the valve
p_s	the pressure of the air source
R	the gas constant
T	absolute temperature of the throttle gas
K_{s3}	the flow rate gain of the flow rate control valve
τ_1	time delay of air supply subsystem

1.0 INTRODUCTION

Supersonic heat-airflow simulated test system (SHSTS) is the basic technical equipment for thermal components test of thermal power machinery, high-speed aircraft and aero engine, and for static and dynamic thermal calibration of high-temperature sensors. It involves basic theories and key technologies such as fluid fuel delivery and control, combustion and temperature control. Its performance level not only directly restricts the development level of national key aero engine but also affects the reliability of static and dynamic calibration of high-temperature sensors and the safety of high-speed aircraft[1,2]. Therefore, the SHSTS is the key supporting equipment to independently develop aero engine and ensure the safety of high-speed aircraft. It is imperative to improve its performance level as one of the basic guarantees for independently developing aero engine. Thermal component test of aero engine and high-speed aircraft, and dynamic thermal calibration of temperature sensor need to produce a uniform and stable temperature field. The uniform and stable temperature field is a direct performance indicator of the SHSTS. The performance of temperature control directly reflects the performance level of the SHSTS[3].

The temperature field of the SHSTS is generated by the combustion of aviation kerosene in high-speed airflow, so the gas temperature of the system is mainly determined by the fuel flow rate and air flow rate which enter the combustor. In theory, as long as the fuel flow rate and air flow rate are accurately controlled, the gas temperature can be accurately controlled. In fact, firstly, in order to achieve high-quality control of gas temperature, fuel flow rate and air flow rate need to maintain a certain proportion; that is, there is a certain requirement for air-fuel ratio. Secondly, the fluctuation of fuel flow rate and air flow rate will change the air-fuel ratio, thus affecting the control quality of gas temperature. This requires not only to maintain a fixed air-fuel ratio in the test process, but also to keep the dynamic characteristics of fuel flow rate in synchronisation with the dynamic characteristics of air flow rate. For example, in a test, when the fuel supply subsystem is disturbed, the fuel flow rate will deviate from the original set value and then return to the original state, meanwhile, the air flow rate is required to have a process from deviation to recovery with the same characteristics in a given proportion, and *vice versa*. Therefore, fuel flow rate and air flow rate are required to be coordinated control, that is to say, fuel flow rate and air flow rate are changed according to a certain proportion. However, in the current control system, fuel flow rate and air flow rate are controlled separately, and they are independent. Therefore, in order to achieve the coordinated control of fuel flow rate and air flow rate, a new control method is needed.

https://doi.org/10.1017/aer.2020.22 Published online by Cambridge University Press

The fuel supply subsystem and air supply subsystem of the SHSTS are characterised by pure time delay due to flow rate sensor and long pipeline, and there are also some characteristics such as time-varying parameters and disturbance in the actual operation process. These characteristics have a negative impact on the high-quality control of fuel flow rate and air flow rate. In order to solve the problem of pure time delay in the system, many scholars had done a lot of theoretical and practical research work and put forward many control methods that can solve this problem. These methods mainly include Smith predictor method[4–6], Dahlin algorithm[7,8], and model prediction algorithm[9–11]. However, the above control methods are only effective for the pure time delay problem but cannot solve the time-varying parameters and disturbance problems in the system. In order to solve the problem of time-varying parameters and disturbance in the system, many effective methods such as sliding mode control[12,13], robust control[14,15] and intelligent control[16–18] were proposed. Subsequently, in order to solve the problems of pure time delay, time-varying parameters and disturbance in the system, many effective methods, such as sliding-mode Smith predictor method[19,20], sliding-mode predictive control algorithm[21,22], robust Smith predictive method[23,24], robust predictive control algorithm[25,26], Smith-fuzzy predictive control algorithm[27,28] and neural Smith predictive method[29,30] had been formed by combining sliding-mode control, robust control and intelligent control with Smith predictor method, and predictive algorithm.

Coordination is a common problem in motion control, such as multi-axis coordinated synchronous control of CNC machine tools, multi-motor synchronous control and large engineering vehicles coordinated control[31,32]. The basic method to solve the above-coordinated control problem is the cross-coupling algorithm. Its basic idea is to calculate the asynchronisation error in real time according to the feedback information of each independent control loop, and to configure the output to each loop according to certain relationship, so as to achieve coordinated synchronisation. In the previous work (see Ref. 2), in order to solve the coordinated control problem of the fuel supply system, the cross-coupling control strategy was used to realise the coordinated control of the fuel flow rate. In this paper, in order to solve the problem of coordinated control of fuel flow rate and air flow rate, a cross-coupling control strategy with fuzzy-PI algorithm was introduced. The basic idea of the algorithm is to introduce the tracking error of fuel flow rate and air flow rate into the forward link through the fuzzy-PI algorithm, and act on the controlled object, so as to realise the dynamic tracking of the two systems, i.e. coordinated control. Therefore, the whole coordination controller consists of a flow rate error tracking controller and a cross-coupling controller.

2.0 SYSTEM MODELING

2.1 Fuel supply subsystem model

Fuel supply subsystem consists of frequency converter, frequency conversion motor, quantitative pump, electro-hydraulic proportional throttle valve, pipeline-valve group and gear flowmeter, which provides aviation kerosene for combustor. Its basic working principle is: when the fuel flow rate required by the system is small, the speed of the frequency conversion pump is fixed, and the fuel flow rate is controlled by adjusting the opening of the proportional throttle valve; when the fuel flow rate required by the system is large, the proportional throttle valve is closed, and the fuel flow rate is controlled by controlling the output frequency of the frequency converter. In order to simplify the problem, this paper only considered the case of large flow rate; that is, frequency conversion pump control mode. Under this working

https://doi.org/10.1017/aer.2020.22 Published online by Cambridge University Press

mode, the fuel supply subsystem is mainly composed of frequency converter, motor, quantitative pump and pipeline, and the bypass proportional valve does not work. The transfer function between the fuel flow rate q_f and the control voltage of the frequency converter can be obtained by referring literature[33].

$$G_{f1}(s) = \frac{q_f(s)}{u(s)} = \frac{b_0}{a_2 s^2 + a_1 s + a_0} \quad \ldots(1)$$

where $b_0 = \frac{1}{60} K_1 K_f K_{int} D_p$; $a_2 = \frac{\pi}{30} J_T C_p L$; $a_1 = \frac{\pi}{30} J_T + K_3 L + \frac{\pi}{30} J_T C_p R + C_p L(K_2 + \frac{\pi}{30} B_T)$; $a_0 = (1 + C_p R) \cdot (K_2 + \frac{\pi}{30} B_T) + K_3 R$; $K_1 = \frac{3 m_p}{2\pi R_{re}} K_f$; $K_2 = \frac{m_p^2}{40\pi R_{re}}$; $K_3 = \frac{D_p^2}{120\pi \eta_m}$; $R = R_L + R_N$; K_f is the gain between the frequency f and control voltage u; K_{int} is the voltage-frequency ratio; m_p is number of the motor pole pairs; R_{re} is equivalent resistance of the rotor; J_T is the rotational inertia of the motor shaft; B_T is damping coefficient of the motor shaft; D_p is displacement of the pump; η_m is the mechanical efficiency of the pump; C_p is the whole leakage coefficient of the fuel circuit; $L = \frac{4\rho_f l}{\pi d^2}$ is liquid inductance; $R_L = \frac{128 \mu l}{\pi d^4}$ is liquid resistance of the pipeline; $R_N = \frac{\sqrt{2\rho_f p_2^*}}{6 C_d A_0}$ is liquid resistance of the nozzle; l is the length of the pipeline; d is the diameter of the pipeline; ρ_f is the fuel density; μ is the dynamic viscosity of the fuel; C_d is flow coefficient of the nozzle; A_0 is the cross-sectional area of the nozzle; p_2^* is the operating spout pressure.

Because the gear flowmeter used in the actual system has the time delay of τ seconds, the actual fuel flow rate q_{sf} obtained during the control will lag τ seconds behind the theoretical fuel flow rate. It can be written as follows.

$$q_{sf}(s) = q_f(s) e^{-\tau s} \quad \ldots(2)$$

2.2 Air supply subsystem model

According to the working principle of the air flow rate supply subsystem, the air flow rate entering the combustor is mainly determined by the opening of the air flow rate control valve, and the valve core displacement of the air flow rate control valve is driven by a set of hydraulic servo system. Therefore, the mathematical models of the hydraulic servo system and the air flow rate control valve are mainly considered when establishing the system model.

(1) Mathematical model of electro-hydraulic servo valve

The electro-hydraulic servo valve consists of servo amplifier and servo valve. The dynamics of servo amplifier can be neglected compared with hydraulic system. Therefore, servo amplifier can be regarded as a proportional link. Therefore, the relationship between its output current and input voltage can be obtained as follows

$$I = K_{s1} u_s \quad \ldots(3)$$

where I is the driving current of the servo valve; K_{s1} is the amplification gain of the servo valve; u_s is the input voltage of the servo amplifier.

When the frequency bandwidth of the servo valve is 3 to 5 times larger than the natural frequency of the system, the servo valve can be considered as a first-order inertial link approximately. Considering that the working frequency of the system is generally not greater

https://doi.org/10.1017/aer.2020.22 Published online by Cambridge University Press

than 30Hz, and the frequency width of the servo valve is generally greater than 100Hz, it can be viewed as a first-order inertia link. The transfer function of the displacement of the servo valve to the input current can be obtained as follows

$$G_{a1}(s) = \frac{x_v(s)}{I(s)} = \frac{K_{s2}}{T_v s + 1} \quad \ldots (4)$$

where x_v is the displacement of the servo valve; K_{s2} is the displacement driving coefficient of the servo valve; T_v is the time constant of the servo valve.

(2) Mathematical model of hydraulic cylinder

Servo-valve-controlled hydraulic cylinder is a typical valve-controlled cylinder system. Its mathematical model can be described by the following three basic equations

$$Q_L = K_{sq} x_v - K_c p_L \quad \ldots (5)$$

$$Q_L = A_p s x_p + \left(\frac{V_t}{4\beta_e} s + C_t \right) p_L \quad \ldots (6)$$

$$A_p p_L = \left(M_t s^2 + B_p s + k_1 \right) x_p + F_L \quad \ldots (7)$$

where K_{sq} is the flow coefficient, K_c is the flow pressure coefficient, p_L is the load pressure, Q_L is the load flow, A_p is the cross-section area of the hydraulic cylinder, C_t is the total leakage coefficient, x_p is the displacement of the piston of the hydraulic cylinder, V_t is the volume of the cylinder block, β_e is the bulk elastic modulus, B_p is the viscous damping coefficient, M_t is the mass of the cylinder block, F_L is the external load force, k_1 is the spring stiffness.

When the elastic load and damping is not considered, the transfer function from piston displacement of hydraulic cylinder to displacement of servo valve can be obtained by Equation (5)–(7):

$$G_{a2}(s) = \frac{x_p(s)}{x_v(s)} = \frac{\frac{K_{sq}}{A_p}}{s\left(\frac{s^2}{\omega_h^2} + \frac{2\zeta_h}{\omega_h} s + 1 \right)} \quad \ldots (8)$$

where $\omega_h = \sqrt{\frac{4\beta_e A_p^2}{M_t V_t}}$ is the hydraulic natural frequency; $\zeta_h = \frac{K_{ce}}{A_p}\sqrt{\frac{\beta_e M_t}{V_t}}$ is the damping ratio; K_{ce}=K_c+C_t is the total pressure and flow coefficient including leakage.

(3) Model of air flow rate control valve

The main function of the air flow rate regulating valve is to regulate the air flow rate into the combustor. The opening of the valve is directly driven by the hydraulic cylinder, so the displacement of the valve is the same as that of the piston of the hydraulic cylinder. In the actual servo control system, the flow process of air is very complex, and the isentropic flow of ideal air through the nozzle is usually used to approximate the flow process. In general, Sanville flow formula is used to calculate the flow rate at the valve port. Therefore, the air mass flow rate into the combustor of the system can be obtained:

https://doi.org/10.1017/aer.2020.22 Published online by Cambridge University Press

$$q_a = C_{d1} w x_p \sqrt{\frac{2}{RT}} p_s f\left(\frac{p}{p_s}\right) \quad \ldots (9)$$

where

$$f\left(\frac{p}{p_s}\right) = \begin{cases} \sqrt{\frac{k}{k-1}\left[\left(\frac{p}{p_s}\right)^{\frac{2}{k}} - \left(\frac{p}{p_s}\right)^{\frac{k+1}{k}}\right]} & 0.528 \le \frac{p}{p_s} \le 1 \\ \left(\frac{2}{k+1}\right)^{\frac{1}{k-1}} \sqrt{\frac{k}{k+1}} & 0 \le \frac{p}{p_s} \le 0.528 \end{cases} \quad \ldots (9)$$

C_{d1} is the flow coefficient of the valve, w is the gradient of the opening area of the valve, p_s is the pressure of the air source, p is the pressure of the combustor, R is the gas constant (287 for air), k is the isentropic index (1.4 for air), and T is the absolute temperature of the throttle gas (set at room temperature).

Because the air from the regulating valve enters into the combustor directly for combustion, there is no obvious load in the system, that is to say the pressure of the gas in the combustor is much less than the pressure of the air source. Therefore, the air mass flow rate entering the combustor through the regulating valve can be approximated as follows:

$$q_2 = K_{s3}\, x_p \quad \ldots (10)$$

where $K_{s3} = \sqrt{\frac{2}{RT}\frac{k}{k+1}}\left(\frac{2}{k+1}\right)^{\frac{1}{k-1}} C_{d1} w p_s$ is defined as the flow rate gain of the flow rate control valve.

(4) Mathematical model of the whole system

The transfer function between the air flow rate and the input voltage of the electro-hydraulic servo-valve amplifier can be obtained by combining Equations (3), (4), (8) and (10).

$$G_a(s) = \frac{q_a(s)}{u_s(s)} = \frac{K_{s1}K_{s2}K_{s3}}{T_v s + 1} \frac{\frac{K_{sq}}{A_p}}{s\left(\frac{s^2}{\omega_h^2} + \frac{2\zeta_h}{\omega_h}s + 1\right)} \quad \ldots (11)$$

In the actual test process, it will take a certain period of time from the time when the servo amplifier is powered on to the time when the air flow rate signal is detected to the computer, so that the system has a pure time delay. Assuming that the pure time delay is τ_1s, the transfer function of the system can be expressed as follows:

$$G_a(s) = \frac{K_{s1}K_{s2}K_{s3}}{T_v s + 1} \frac{\frac{K_{sq}}{A_p}}{s\left(\frac{s^2}{\omega_h^2} + \frac{2\zeta_h}{\omega_h}s + 1\right)} e^{-\tau_1 s} \quad \ldots (12)$$

3.0 CONTROL STRATEGY

3.1 Flow rate control strategy

In order to solve the problems of pure time delay, time-varying parameters and disturbance that are not conducive to accurate control in fuel supply subsystem and air supply subsystem,

https://doi.org/10.1017/aer.2020.22 Published online by Cambridge University Press

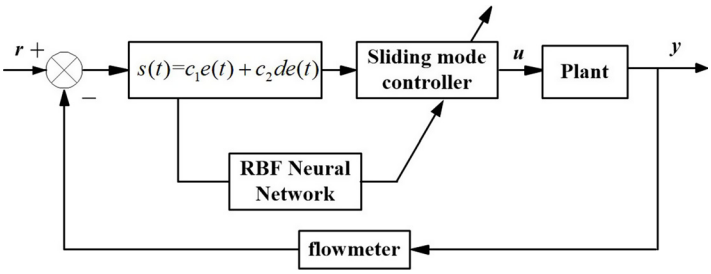

Figure 1. Controller structure.

a neural sliding mode predictive control algorithm based on RBF neural network was proposed in this paper, which combines intelligent control, sliding mode control and predictive control. The controller structure is shown in Fig. 1. The core idea of the algorithm is to use Levinson predictor to solve the problem of pure time delay in the system, use sliding mode control algorithm to solve the problem of time-varying parameters and disturbance in the system, and use RBF neural network to improve the bucket vibration phenomenon in sliding mode control.

(1) Design of sliding mode controller-based RBF neural network

Suppose that the state equation of the controlled object is

$$\dot{x} = Ax + Bu \quad \ldots(13)$$

Assuming that the control instruction is $r(t)$, and the sliding mode switching function is designed as follows:

$$s(t) = c_1 e(t) + c_2 de(t) + \cdots + c_{n-1} d^{(n-2)} e(k) + d^{(n-1)} e(t) \quad \ldots(14)$$

where

$$e(t) = r(t) - x_1 \quad \ldots(15)$$

$$de(t) = dr(t) - x_2 \quad \ldots(16)$$

$$\vdots$$

$$d^{(n-1)} e(t) = d^{(n-1)} r(t) - x_n \quad \ldots(17)$$

Assuming that $X = [x_1, x_1 \cdots x_n]^T$ is the input of RBF neural network, $H = [h_1, h_2 \cdots h_j \cdots h_m]^T$ is the output of hidden layer and h_j is the Gauss function, then

$$h_j = \exp\left(-\frac{\|X - C_j\|^2}{2b_j^2}\right) \quad j = 1, 2, \cdots, m \quad \ldots(18)$$

https://doi.org/10.1017/aer.2020.22 Published online by Cambridge University Press

where $C_j = [c_{j1} \cdots c_{jn}]^T$, $b_j = [b_{j1} \cdots b_{jn}]^T$, m is the number of hidden layer.

Assuming that the weight vector of the network is $W = [w_1, w_2 \cdots w_j \cdots w_m]^T$, then the output of the network is

$$u = w_1 h_1 + w_2 h_2 + \cdots + w_m h_m \quad \ldots (19)$$

Using sliding mode switching function $s(t)$ as the input of RBF neural network and output of RBF neural network as the output of sliding mode controller, the following result can be obtained.

$$u = \sum_{j=1}^{m} w_j \exp\left(-\frac{\|s - c_j\|^2}{2b_j^2}\right) \quad \ldots (20)$$

Since the control objective is to make $s(t)\dot{s}(t) \to 0$, the weight adjustment objective function of RBF network can be set as follows:

$$E = s(t)\dot{s}(t) \quad \ldots (21)$$

Therefore, according to the gradient descent method, the weight learning algorithm of the neural network can be obtained:

$$dw_j = -\frac{\partial E}{\partial w_j(t)} = -\frac{\partial s(t)\dot{s}(t)}{\partial w_j(t)} = -\frac{\partial s(t)\dot{s}(t)}{\partial u(t)}\frac{\partial u(t)}{\partial w_j(t)} \quad \ldots (22)$$

Because

$$\frac{\partial s(t)\dot{s}(t)}{\partial u(t)} = s(t)\frac{\partial \dot{s}(t)}{\partial u(t)} = -s(t) \quad \ldots (23)$$

$$\frac{\partial u(t)}{\partial w_j(t)} = \exp\left(-\frac{\|s - c_j\|^2}{2b_j^2}\right) \quad \ldots (24)$$

so

$$dw_j = s(t)\exp\left(-\frac{\|s - c_j\|^2}{2b_j^2}\right) = s(t)h_j \quad \ldots (25)$$

$$w_j(t) = w_j(t-1) + \eta dw_j + \alpha[w_j(t-1) - w_j(t-2)] \quad \ldots (26)$$

where η is the learning rate, α is the inertia coefficient.

(2) Levinson predictor

Levinson predictor is a method of predicting future d-step output variables by using historical data from simple moving average process. Suppose the output of predictor at k-time is

$$y_m(k) = -\sum_{i=1}^{n} a_i y(k-i) \quad \ldots (27)$$

https://doi.org/10.1017/aer.2020.22 Published online by Cambridge University Press

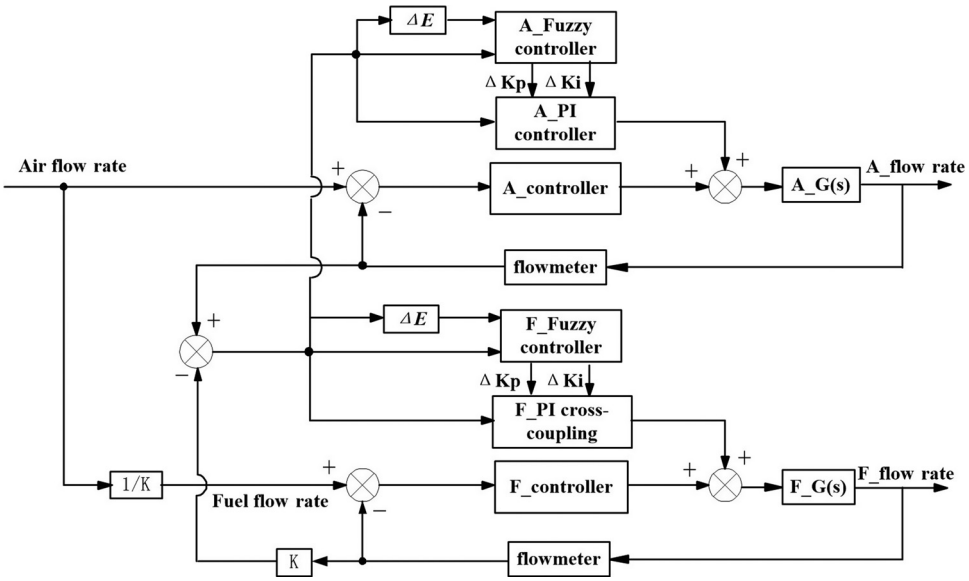

Figure 2. Principle of cross-coupling control strategy based on fuzzy-PI algorithm.

then the predicted value of d-step ahead can be obtained

$$y_m(k+d|k) = -a_1 y_m(k+d-1|k) - \cdots - a_{p-1} y_m(k+1|k) - a_p y(k) - \cdots - a_n y(k+d-n) \quad \ldots (28)$$

The parameters $\{a_i\}$ in Equations (27) and (28) are the best predictive parameters. Usually, after the historical data of system output $\{y(k-1), y(k-2), \cdots y(k-n)\}$ are obtained offline, the parameters can be estimated and determined by Levinson-Durbin algorithm.

3.2 Coordinated control strategy

In order to achieve the coordinated control of fuel flow rate and air flow rate, cross-coupling control strategy based on fuzzy-PI algorithm was introduced. The tracking error of fuel flow rate and air flow rate was introduced into the forward link through the fuzzy PI algorithm, which acted on the controlled object, thus realizing the dynamic tracking of the two-channel flow rate, i.e. coordinated control. The principle of cross-coupled based on fuzzy-PI algorithm is shown in Fig. 2. It can be seen from the figure that the principle of the algorithm is to change the output of controller by adjusting the PI parameters of cross-coupled links, so as to improve the tracking effect of fuel flow rate and air flow rate. Here the input of the fuzzy controller is the error between the actual feedback value of fuel flow rate and air flow rate and its rate of change.

Because we have some prior knowledge, the input of the two fuzzy controllers are error and the rate of error change, and the output are the variation of PI parameters ΔK_p and ΔK_I. At the beginning of operation, the system has PI parameters ΔK_{p0} and ΔK_{I0} which have been preset. The output variation of the fuzzy controller will be directly added to the original PI parameters.

https://doi.org/10.1017/aer.2020.22 Published online by Cambridge University Press

Table 1
Fuzzy control rules

E \ ΔE	NB	NM	NS	ZO	PS	PM	PB
NB	NB	NB	NM	NM	NS	ZO	ZO
NM	NB	NB	NM	NS	NS	ZO	ZO
NS	NB	NM	NS	NS	ZO	PS	PS
ZO	NM	NM	NS	ZO	PS	PM	PM
PS	NM	NS	ZO	PS	PS	PM	PB
PM	ZO	ZO	PS	PS	PM	PB	PB
PB	ZO	ZO	PS	PM	PM	PB	PB

Table 2
Model parameters of fuel supply subsystem

Parameter	Value	Parameter	Value
$R_2^{'}/\Omega$	7.56	A/m^2	8.478×10^{-6}
$J_\mathrm{T}/(\mathrm{kg}\cdot\mathrm{m}^2)$	0.054	l/m	12
$B_\mathrm{T}/(\mathrm{N}\cdot\mathrm{m}\cdot\mathrm{s}\cdot\mathrm{rad}^{-1})$	0.045	d/m	0.01
$C_\mathrm{p}/(\mathrm{m}^3\cdot\mathrm{Pa}\cdot\mathrm{s}^{-1})$	9.25×10^{-11}	τ/s	3
$\mu/(\mathrm{N}\cdot\mathrm{s}\cdot\mathrm{m}^{-2})$	2.34×10^{-3}	C_d	0.6
$D_\mathrm{p}/(\mathrm{m}^3\cdot\mathrm{r}^{-1})$	20×10^{-6}	η_m	0.87
$\rho_\mathrm{oil}/(\mathrm{Kg}\cdot\mathrm{m}^{-3})$	7.8×10^2	m_p	3

In this paper, the domains of ΔK_p and ΔK_I in fuzzy-PI cross coupling controller of fuel flow rate are $(-0.02, 0.02)$ and $(-0.05, 0.05)$, respectively. The domains of ΔK_p and ΔK_I in fuzzy-PI cross coupling controller of air flow rate are $(-0.05, 0.05)$ and $(-0.01, 0.01)$ respectively. The domains of two-channel flow rate error are $(-1.0, 1.0)$ and the domains of error variation are $(-1.0, 1.0)$.

Both fuzzy controllers adopted the same fuzzy control rules; it can be seen in Table 1.

4.0 SIMULATION

4.1 Simulation parameters

According to the mathematic model established in previous section, the simulation model was built in Matlab. The simulation parameters were obtained by looking up tables and calculating, and they are shown in Tables 2 and 3.

4.2 Single channel flow rate control simulation

Accurate control of single-channel flow rate is the premise of realising coordinated control of double-channel flow rate. Therefore, this paper first used the proposed neural sliding mode

https://doi.org/10.1017/aer.2020.22 Published online by Cambridge University Press

Table 3
Model parameters of air supply subsystem

Parameter	Value	Parameter	Value
$K_{s1}/(\mathrm{A}\cdot\mathrm{V}^{-1})$	0.3	A_p/m^2	0.002
$K_{s2}/(\mathrm{m}\cdot\mathrm{A}^{-1})$	0.00033	M_t/kg	5.5
$K_{sq}/(kg\cdot m^{-1}s^{-1})$	0.048	V_t/m^3	0.003
$R/(\mathrm{J}\cdot kg^{-1}\mathrm{K}^{-1})$	287	β_e/Pa	680×10^6
T/K	300	$K_{ce}/(\mathrm{m}^3\cdot\mathrm{Pa}\cdot\mathrm{s}^{-1})$	6.25×10^{-10}
k	1.4	τ_1/s	1
T_v/s	0.5	P_s/Pa	1×10^6
$C_{\mathrm{d}1}$	0.6	W/m	0.0785

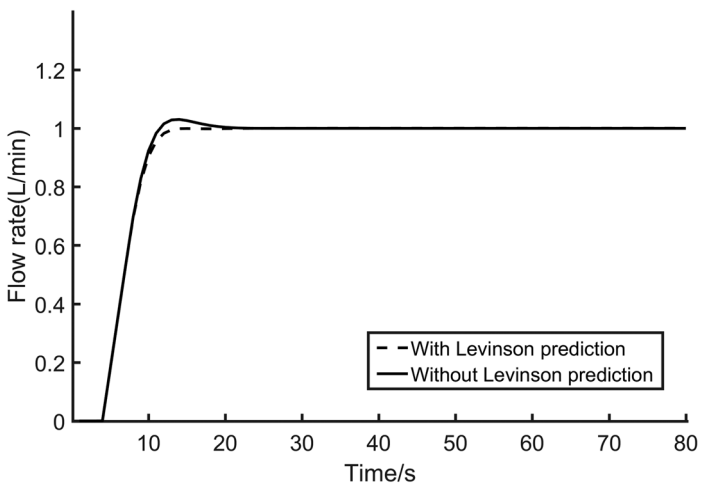

Figure 3. Control results of fuel flow rate with and without predictor.

predictive control algorithm to simulate the control of single-channel flow rate. In order to illustrate the control effect of the proposed control algorithm directly and clearly, the effectiveness of the control algorithm was only illustrated by the simulation results of fuel flow rate. In the simulation, the control period is 1s, and the target fuel flow rate is 1L/min. The parameters of the neural sliding mode controller are $m=5$, $C=[-3, -1.5, 0, 1.53]$, $b=2$, and the advanced prediction step of Levinson predictor is five steps, the order of the predictor is six. The optimal parameters are $\{-1.1159, 0.0826, 0.0237, 0.0068, 0.0019, 0.00086\}$. In order to show the effect of the proposed neural sliding mode predictive control algorithm on the suppression of pure time delay, the fuel flow rate control simulation was carried out with and without predictor under the same simulation parameters. The simulation results are shown in Fig. 3. It can be seen from the figure that in the case of with predictor, fuel flow rate can be controlled quickly and accurately without overshoot, while in the case of without predictor, fuel flow rate appears overshoot, which shows that the setting of predictor is effective to compensate for the pure time delay of the system.

From the modeling process of system mentioned above, it can be seen that the parameters of the system have time-varying characteristic. In order to verify the ability of the controller

https://doi.org/10.1017/aer.2020.22 Published online by Cambridge University Press

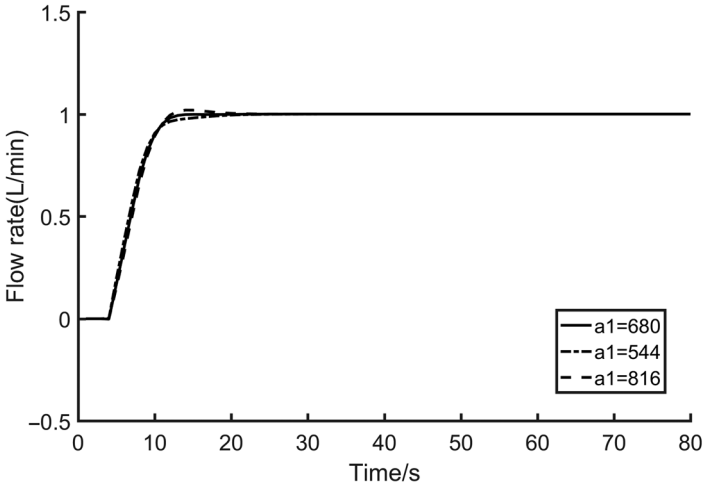

Figure 4. Control results of fuel flow rate under model parameters changing.

designed in this paper to overcome the time-varying parameters, the control simulation of the fuel flow rate was carried out by using the proposed control algorithm under the condition that the model parameters have changed and the control parameters remain unchanged. In the simulation, the target fuel flow rate is still 1L/min, the simulation results were carried out when the parameter a_1 of the fuel supply subsystem increased by 20% ($a_1 = 816$) and decreased by 20% ($a_1 = 544$), and the simulation results are shown in Fig. 4. The simulation results show that although the control effect will be slightly worse when the system parameters have changed, the overall control effect can still be maintained. This shows that the control algorithm designed in this paper has the ability to overcome the time-varying parameters of the system.

In order to verify the anti-jamming capability of the proposed control algorithm, a simulation study was carried out under the condition that a voltage disturbance is added to the system at the 50^{th} second of the system response, and the other parameters of the controller remain unchanged. Figure 5 is the simulation results by using the proposed control algorithm when 0.1V and −0.1V disturbances were added to the control system, respectively. It can be seen from the figure that when disturbance is added to the system, the response of the system will be obviously affected; that is, the control curve deviates from the original state and overshoots occur, but under the action of the controller, the response curve of the system quickly restores to the original state, which shows that the neural sliding mode predictive control algorithm designed in this paper can be very good. It can overcome the disturbance in the system and achieve the predetermined goal of the control system.

4.3 Coordination control simulation

According to the analysis of the previous section, in order to ensure the high quality control of gas temperature of the SHSTS, besides maintaining the optimum proportion of fuel flow rate and air flow rate, the dynamic characteristics of fuel flow rate and air flow rate should be synchronized; that is, the fuel flow rate and air flow rate should be controlled coordinately. In order to achieve the coordinated control of fuel flow rate and air flow rate, the closed-loop

https://doi.org/10.1017/aer.2020.22 Published online by Cambridge University Press

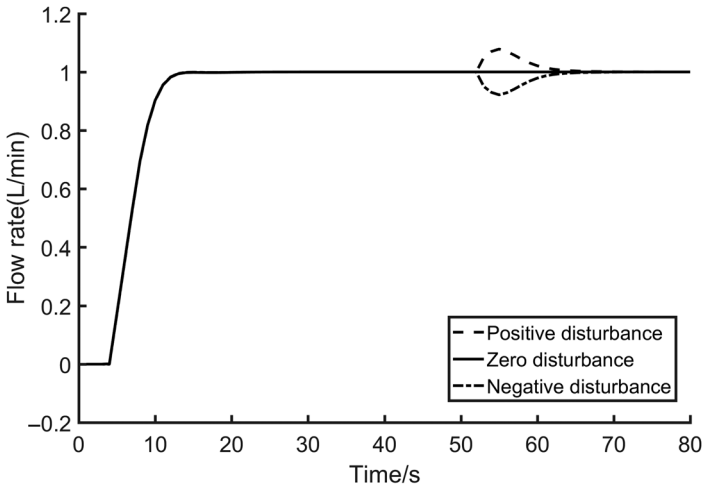

Figure 5. Control results of fuel flow rate under disturbance.

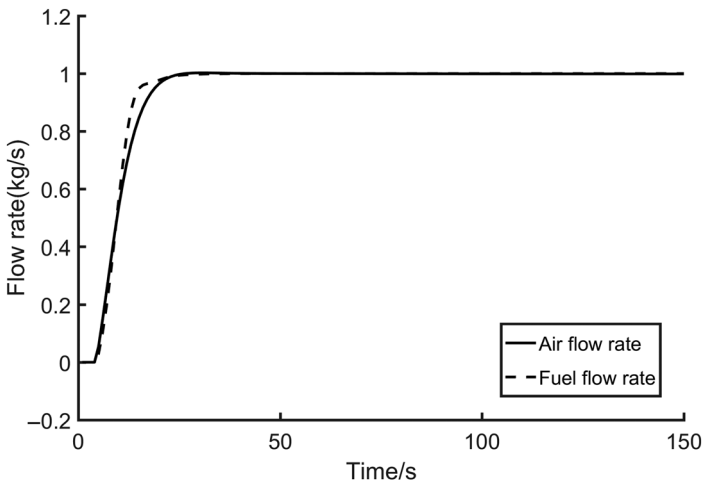

Figure 6. The response curves of fuel flow rate and air flow rate tend to be consistent.

response curves of fuel flow rate and air flow rate should be basically the same. Therefore, the response curves of fuel flow rate and air flow rate were basically consistent by adjusting the control parameters; it can be seen in Fig. 6. In order to ensure the optimum combustion ratio of fuel (aviation kerosene) to air (1:14.7), the fuel flow rate was set to 0.068kg/s and the air flow rate was set to 1kg/s in simulation. In order to make the response of the two flow rates consistent and easy to compare, the simulation data of fuel flow rate was multiplied by 14.7, and the simulation results can be found in Fig. 6. It can be seen from the figure that the closed-loop response curves of fuel flow rate and air flow rate are basically the same by adjusting the control parameters, which lay a solid foundation for the coordinated control of fuel flow rate and air flow rate.

https://doi.org/10.1017/aer.2020.22 Published online by Cambridge University Press

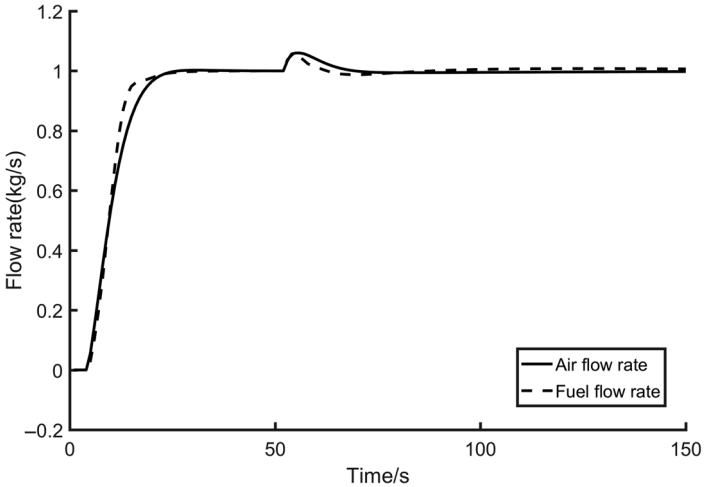

Figure 7. Coordinated control result when air supply subsystem with disturbance.

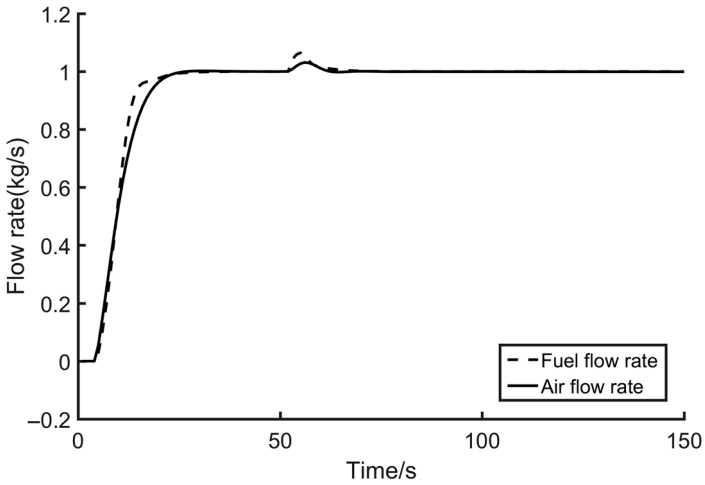

Figure 8. Coordinated control result when fuel supply subsystem with disturbance.

In order to verify that the proposed control algorithm can achieve the coordinated control of fuel flow rate and air flow rate, the coordinated control of fuel flow rate and air flow rate was simulated in two cases. In the first case, when the air supply subsystem was disturbed at the 50th second of the simulation control and the change of fuel flow rate with air flow rate was observed; in the second case, when the fuel supply subsystem was disturbed at the 50th second of the simulation control and the change of air flow rate with fuel flow rate was observed. The simulation results are shown in Figs 7 and 8. It can be seen from the figures that when the air flow rate response curve fluctuates due to the system interference, the fuel flow rate will fluctuate accordingly, that is to say, the fuel flow rate can change with the change of

https://doi.org/10.1017/aer.2020.22 Published online by Cambridge University Press

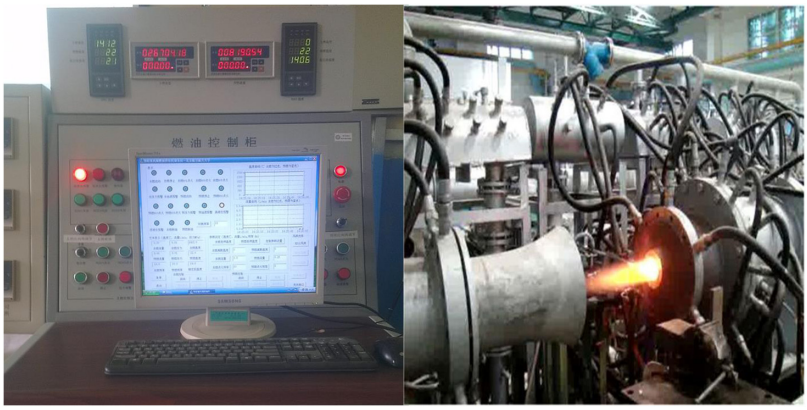

Figure 9. Experimental equipment.

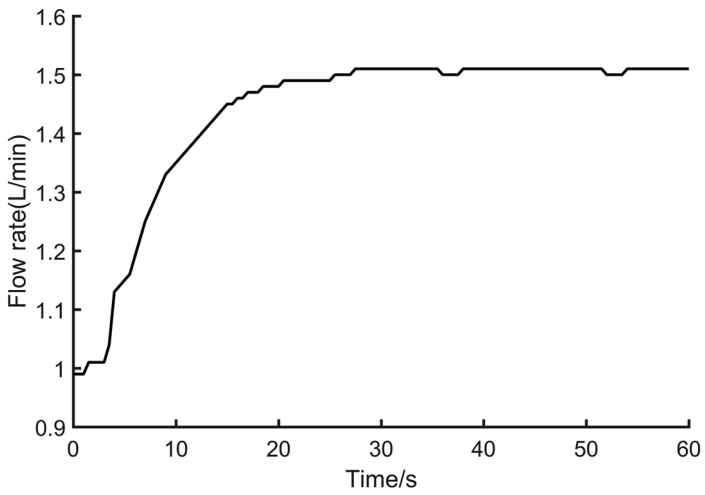

Figure 10. Control result of fuel flow rate.

the air flow rate; conversely, when the fuel flow rate response curve fluctuates due to the system interference, the air flow rate can also follow. Therefore, the cross-coupling coordinated controller designed in this paper is effective and can realize the coordinated control of fuel flow rate and air flow rate.

5.0 EXPERIMENT

5.1 Experimental equipment

In order to realise the control of fuel flow rate and air flow rate of the SHSTS and their coordinated control, based on the existing hardware of fuel supply subsystem and air supply subsystem, the measurement and control system based on the field PLC controller and remote industrial computer was developed. The experimental equipment is shown in Fig. 9.

https://doi.org/10.1017/aer.2020.22 Published online by Cambridge University Press

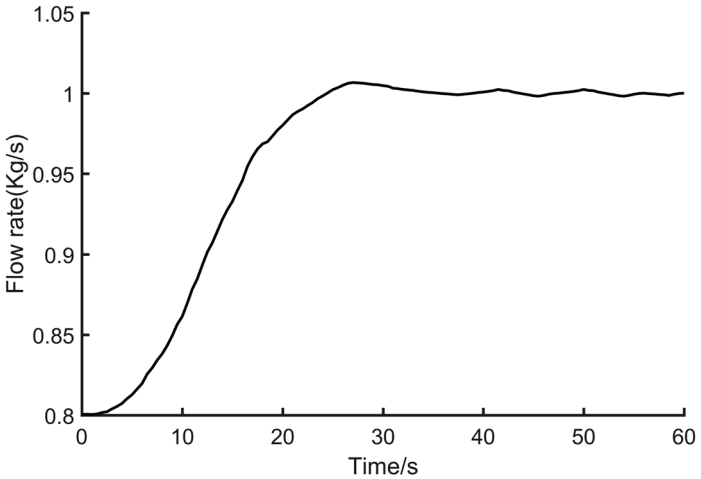

Figure 11. Control result of air flow rate.

5.2 Single channel flow rate control experiment

Because the precise control of fuel flow rate and air flow rate is the basis of realising the coordinated control of them, it is necessary to study the separate control of fuel flow rate and air flow rate firstly. In the experiment, the fuel flow rate and air flow rate were adjusted to a fixed value firstly, and then step response experiments were carried out. The experimental results are shown in Figs 10 and 11. It can be seen from the figures that the system runs smoothly with no overshoot and the absolute control precision is ± 0.01L/min in the process of the fuel flow rate stepping from 1L/min to 1.5L/min, which meets the predetermined control requirements. In the process of air flow rate stepping from 0.8kg/s to 1.0kg/s, the system achieves a good control effect, that is, the air flow rate is smoothly controlled without overshoot, and the control accuracy is ± 2.5g/s.

5.3 Coordinated control experiment

In order to verify the effectiveness of the proposed coordinated control algorithm of fuel flow rate and air flow rate, the coordinated control experiment of fuel flow rate and air flow rate was completed. The control method used in the actual experiment is the same as the control algorithm used in the simulation, that is, the neural sliding mode predictive control algorithm and cross-coupling control were used to complete the coordinated control experiment. The experimental results are shown in Fig. 12. The setting value of fuel flow rate and air flow rate in the experiment are the same as those in the simulation, i.e. the air flow rate is 1.0kg/s and the fuel flow rate is 0.068kg/s. In the experiment, the two-channel flow rates were adjusted to the target flow rate, and then a disturbance was added to the air supply subsystem during the experiment, that is to say, the air flow rate will fluctuate upward and recover. The experimental results show that the change of air flow rate will lead to the change of fuel flow rate when the coordinated control is added, that is to say, the coordinated control of two-channel flow rates is realized. In addition, because the absolute error of fuel flow rate is about ± 0.5g/s in the experiment, if multiplied by 14.7, the error will be magnified by 14.7 times, so the fuel flow rate is not multiplied by 14.7 times.

https://doi.org/10.1017/aer.2020.22 Published online by Cambridge University Press

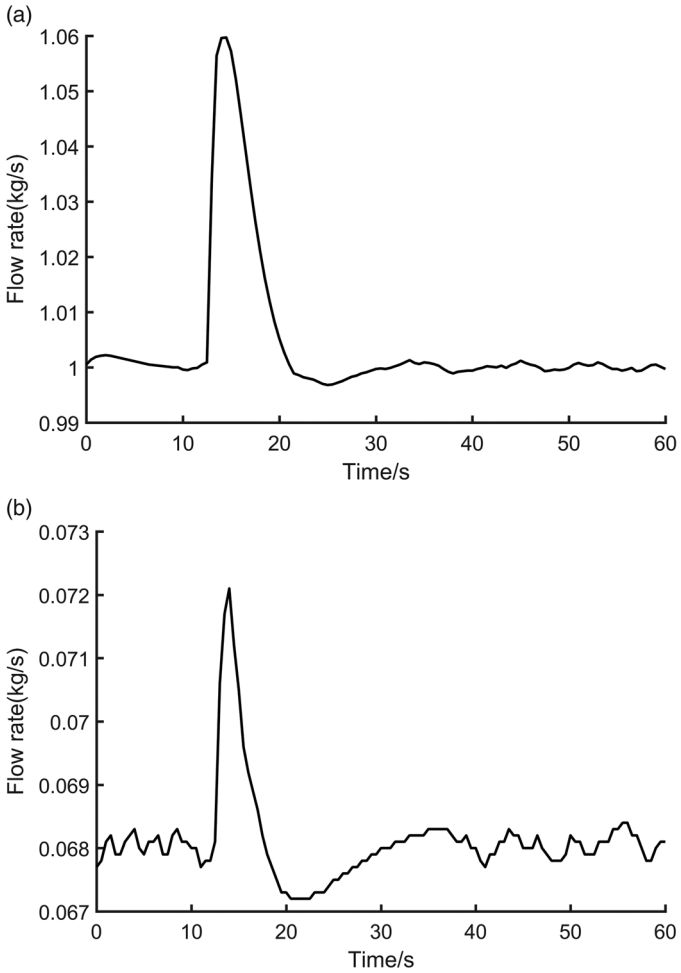

Figure 12. Coordinated control result of fuel flow rate and air flow rate.

6.0 CONCLUSIONS

Aiming at the problem of coordinated control of fuel flow rate and air flow rate of the SHSTS, the mathematical models of fuel supply subsystem and air supply subsystem are established, and the characteristics of the system are analysed on this basis. According to the characteristics of the system and the requirements of coordinated control, a cross-coupling coordinated control strategy based on neural sliding mode predictive control is proposed, which uses neural sliding mode predictive control to achieve accurate control of fuel flow rate and air flow rate, and uses cross-coupling to achieve coordinated control of the two. On this basis, the proposed control algorithm is simulated and experimentally studied, and the following conclusions are drawn:

(1) The proposed neural sliding mode predictive control algorithm has the capability to overcome the pure time delay, time-varying parameters and interference of the system. It can

https://doi.org/10.1017/aer.2020.22 Published online by Cambridge University Press

achieve a fast without overshoot control of fuel flow rate and air flow rate, and the control accuracy meets the requirements of the system.

(2) The proposed cross-coupled coordinated control algorithm can achieve the coordinated control between fuel flow rate and air flow rate, and a satisfactory control effect is obtained.

FUNDING

This work was supported by the Nature Science Foundation of Hebei Province grant no. E2017402037, and science and technology research project of Hebei Province, grant no. ZD2018012.

REFERENCES

1. CAI, C., MA, Q., WU, D. and FAN, L. Design and implementation of the fuel supply for the high-temperature combustion System, *Adv Mech Eng*, 2017, **9**, (1), pp 1–8.
2. CAI, C., YANG, Y. and LIU, T. Coordinated control of fuel flow-rate for a high-temperature high-speed wind tunnel, *Proc Inst Mech Eng Part G- J Aerosp Eng,* 2016, **230**, (13), pp 2504–2514.
3. FAN, L., CAI, C. and WU, B. Modeling and simulation of gas temperature in high speed hot air flow simulation test system, *China Sci Paper*, 2015, **10**, (23), pp 2745–2748.
4. MATAUSEK, M.R. and MICIC, A.D. A modified Smith predictor for controlling a process with an integrator and long dead-time, *IEEE Trans Autom Cont*, 1996, **41**, (8), pp. 1199–1203.
5. MATAUSEK, M.R. and MICIC, A.D. On the modified Smith predictor for controlling a process with an integrator and long dead-time, *IEEE Trans Autom Cont*, 1999, **44**, (8), pp 1603–1606.
6. ASTROM, K.J., HANG, C.C. and LIM, B.C. A new Smith predictor for controlling a process with an integrator and long dead-time, *IEEE Trans Autom Cont*, 1994, **39**, (2), pp 343–345.
7. DEHLIN, E.B. Designing and tuning digital controllers, *Instr Contr Sys*, 1968, **41**, (7), pp 77–79.
8. ZHU, X.F. Dalin algorithm research, *Chemical Autom Inst*, 1989, **14**, (5), pp 23–27.
9. KWON, W.H., LEE, Y.S. and HAN, S.H. General receding horizon control for linear time-delay systems, *Automatic*, 2004, **40**, (9), pp 1603–1611.
10. RODRIGUES, J.A.D. and MACIEL FILHO, R. Application of a novel approach for DMC predictive controller design by response surface analysis in a fed-batch bioreactor, *Comput Chem Eng*, 1999, **23**, (1), pp S293–S296.
11. RODRIGUES, J.A.D., TOLEDO, E.C.V. and MACIEL FILHO, R. A tuned approach of the predictive–adaptive GPC controller applied to a fed-batch bioreactor using complete factorial design, *Comput Chem Eng*, 2002, **26**, (10), pp 1493–1500.
12. WU, L., SU, X. and SHI, P. Sliding mode control with bounded gain performance of Markovian jump singular time-delay systems, *Automatic*, 2012, **48**, (8), pp 1929–1933.
13. KHANDEKAR, A.A., MALWATKAR, G.M. and PATRE, B.M. Discrete sliding mode control for robust tracking of higher order delay time systems with experimental application, *ISA Trans*, 2013, **52**, (1), pp 36–44.
14. ZHOU, K., PRAMOD, P.K., JAKOB, S. and HANS, H.N. Robust performance of systems with structured uncertainties in state space, *Automatic*, 1995, **31**, (2), pp 249–255.
15. JABBARI, F. and SCHMITENDORF, W.E. Robust linear controllers using observers, *IEEE Auto Cont*, 1991, **36**, (12), pp 1509–1514.
16. INDRANIL, P., SAPTARSHI, D. and AMITAVA, G. Tuning of an optimal fuzzy PID controller with stochastic algorithms for networked control systems with random time delay, *ISA Trans*, 2011, **50**, (1), pp 28–36.
17. JING, N.A., REN, X. and HUANG, H. Time-delay positive feedback control for nonlinear time-delay systems with neural network compensation, *Acta Automatica Sinica*, 2008, **34**, (9), pp 1196–1203.
18. KWON, O., PARK, J.H., LEE, S.M. and CHA, E.J. Analysis on delay-dependent stability for neural networks with time-varying delays, *Neurocomputing,* 2013, **103**, pp 114–120.

https://doi.org/10.1017/aer.2020.22 Published online by Cambridge University Press

19. UTKAL, M. and Ibrahim, K. Smith predictor with sliding mode control for processes with large dead times, *J. Electric Eng,* 2017, **68**, (6), pp 463–469.
20. UTKAL, M. and RUBÉN, R. Smith predictor based sliding mode control for a class of unstable processes, *Transactions of the Institute of Measurement and Control*, 2017, **39**, (5), pp 706–714.
21. SHEN, W., PAN, Z., LI, M. and PENG, H. Lateral control method for wheel-footed robot based on sliding mode control and steering prediction, *IEEE Access*, 2018, **6**, pp 58086–58095.
22. XU, Q.S. Digital integral terminal sliding mode predictive control of piezoelectric-driven motion system, IEEE Trans Ind Electron 2016, 63, (6), pp 3976–3984.
23. LEE, T.H, WANG, Q.G. and TAN, K.K. Robust smith-predictor controller for uncertain delay systems, *AIChE J*, 1996, **42**, (4), pp 1033–1040.
24. STOJIC, M.R., MATIJEVIC, F.S. and DRAGANOVIC, L.S. A robust Smith predictor modified by internal models for integrating process with dead time, *IEEE Trans Autom Cont*, 2001, **46**, (8), pp 1293–1298.
25. RINCON, L., CORONADO, E., HENDRA, H. et al. Expressive states with a robot arm using adaptive fuzzy and robust predictive controllers, *3rd International Conference on Control and Robotics Engineering*, April, 2018, Nagoya, Japan.
26. WANG, Y., PEÑA, D.M., PUIG, V. and CEMBRANO, G. Robust economic model predictive control based on a periodicity constraint, *Int J Robust Nonlinear Cont*, 2019, **29**, pp 3297–3309.
27. WEI, Q. and WANG, W. Research on fuzzy self-adaptive PI-Smith control in long time-delay system, *J China UnivPosts Telecommun*, 2011, **18**, (5), pp 114–117.
28. MARUSAK, P.M. Advantages of an easy to design fuzzy predictive algorithm in control systems of nonlinear chemical reactors, *Appl Soft Comput*, 2009, **9**, (3), pp 1111–1125.
29. HUANG, J., LEWIS, F.L. and LIU, K. A neural net predictive control for telerobots with time delay. *J Intell Robot Syst*, 2000, **29**, pp 1–25.
30. TAN, Y.H. and CAUWENBERGHE, V. Neural network based on nonlinear smith predictor, *Control Theory and Applications*, 2000, **17**, (3), pp 410–414.
31. KOREN, Y. Cross-couple bixial computer control for manufacturing systems, *J Dyn Syst Meas Cont*, 1980, **102**, (4), pp 265–272.
32. KERON, Y. and LO C.C. Advanced controllers for feed drives, *Ann CIRP*, 1992, **41**, pp 689–698.
33. LI Y. CAI C, LEE K and TENG F. A novel cascade temperature control system for a high-speed heat-airflow wind tunnel, *IEEE/ASME Trans Mechatron* 2013, **18**(4), 1310–1319.

https://doi.org/10.1017/aer.2020.22 Published online by Cambridge University Press